A Tensor-Based Data-Driven Approach for Multidimensional Harmonic Retrieval and Its Application for MIMO Channel Sounding

Yanming Zhang, *Member, IEEE*, Wenchao Xu, *Member, IEEE*, A-Long Jin, *Member, IEEE*, Min Li, *Member, IEEE*, Ping Yuan, *Student Member, IEEE*, Lijun Jiang, *Fellow, IEEE*, and Steven Gao, *Fellow, IEEE*

***Abstract*—In wireless channel sounding, accurately estimating multiple parameters within a multipath signal, such as azimuth, elevation, Doppler shift, and delay, necessitates addressing the challenges posed by the multidimensional harmonic retrieval (MHR) problem. To overcome these complexities, we propose a framework based on high-order dynamic mode decomposition (HODMD) that designed for robustly estimating frequencies of interest from high-dimensional sinusoidal signals, particularly in additive white Gaussian noise conditions. The HODMD approach, a hybrid algorithm amalgamating high-order singular value decomposition (HOSVD) and dynamic mode decomposition (DMD), operates by initially decomposing observed tensorial data into a core tensor and R mode matrices through HOSVD. Subsequently, DMD is applied to analyze each mode matrix individually, decomposing it into dynamic modes and DMD eigenvalues. The imaginary component of the DMD eigenvalues yields frequencies along the rth dimension. By uniformly applying this analysis to all mode matrices, multiple frequencies of interest are efficiently obtained. Furthermore, the integration of HOSVD, DMD, and moving average techniques in the proposed method is designed to mitigate noise interference during the MHR process. We conduct several numerical experiments and present a real-life example, i.e., the double-direction multiple-input and multiple-output (MIMO) channel sounding, to validate the effectiveness of the proposed HODMD approach. Results demonstrate that HODMD outperforms comparable approaches, particularly in scenarios characterized by high-signal-to-noise ratios. Notably, the proposed method exhibits the capability to estimate the number of tones in undamped cases during the decomposition process. Hence, our work contributes a practical and effective tensor-based solution to the MHR problem, particularly in the context of channel parameter estimation for MIMO systems.**

***Index Terms*—Data-driven approach, double-directional multiple-input and multiple-output (MIMO) channel sounding, high-order dynamic mode decomposition (HODMD), multidimensional harmonic retrieval (MHR).**

Received 23 July 2024; revised 31 August 2024; accepted 1 October 2024. Date of publication 7 October 2024; date of current version 24 January 2025. This work was supported in part by the Chinese University of Hong Kong Startup Fund under Grant 4937123, Grant 4937124, Grant 14223422, and Grant 14201923; in part by the Research Grants Council of the Hong Kong Special Administrative Region under Project PolyU15225023; in part by the Research Grants Council of Hong Kong under Grant GRF 14210623; in part by Innovation and Technology Fund Grant ITP/007/23LP; in part by Hong Kong University Grants Committee under Grant AoE/E-603/18; and in part by the General Program of the National Natural Science Foundation of China under 62471332. *(Corresponding author: A-Long Jin.)*

Yanming Zhang and Steven Gao are with the Department of Electronic Engineering, The Chinese University of Hong Kong, Hong Kong, China (e-mail: ymzhang@eee.hku.hk; scgao@ee.cuhk.edu.hk).

Wenchao Xu is with the Department of Computing, The Hong Kong Polytechnic University, Hong Kong, China (e-mail: wenchao.xu@polyu.edu.hk).

A-Long Jin is with the Department of Communications and Networking, Xi'an Jiaotong-Liverpool University, Suzhou 215000, China (e-mail: along.jin@xjtlu.edu.cn).

Min Li is with the School of Microelectronics, Tianjin University, Tianjin 300200, China (e-mail: minli@eee.hku.hk).

Ping Yuan is with the Department of Electrical and Electronic Engineering, The University of Hong Kong, Hong Kong, China (e-mail: yuanp019@connect.hku.hk).

Lijun Jiang is with the Department of Electrical and Computer Engineering, Missouri University of Science and Technology, Rolla, MO 65409 USA (e-mail: ljf82@mst.edu).

Digital Object Identifier 10.1109/JIOT.2024.3474916

I. Introduction

MULTIDIMENSIONAL harmonic retrieval (MHR) problems often appear in the context of multiple-input and multiple-output (MIMO) wireless channel sounding [1]. For instance, five parameters, including the direction-of-arrival (DOA), direction-of-departure (DOD), Doppler shift, propagation delay, and complex path loss, are comprised in the double-directional MIMO model [2]. These parameters are typically determined by fitting models to measurements obtained during channel sounding campaigns, where the estimation of signal parameters boils down to MHR [1], [3], [4]. The relevance of MHR extends significantly into the Internet of Things (IoT) field, particularly in applications, such as the Internet of Vehicles (IoV) [5], unmanned aerial vehicle localization [6], and smart sensor networks [7].

Often, an R-dimensional (R-D) harmonic signal constructed by sampling along an R-D regular grid can be regarded as a tensor-based generalization of the 1-D harmonic one [8]. When performing harmonic retrieval on such a signal, a large number of frequencies need to be evaluated [9]. Specifically, estimating frequencies from an R-D harmonic signal with I tones requires deriving $R \times I$ parameters [10]. To this end, various retrieval methods are proposed, such as canonical polyadic decomposition (CPD) [9], [11], tensor-train decomposition (TTD) [12], [13], [14], singular value decomposition (SVD) [15], [16], high-order SVD (HOSVD) [17], [18], etc. To summarize, we have classified the seminal contributions into two categories, namely, matrix-based schemes and tensor-based schemes. For the matrix-based scheme, estimation of signal parameters via rotational invariance techniques (ESPRITs) [19] and multiple

signal classification (MUSIC) [20], [21] are two classical algorithms for signal parameter estimation that analyze the vector or matrix form of the sampled data. In order to apply these methods to the MHR problem, the observed tensorial data can be reshaped into the corresponding vector or matrix representation. ESPRIT has been extended into 2-D [22], 3-D [23], and R-D forms [24]. Similarly, MUSIC is modified into the decoupled root [25] and augmented tensor [26] form by rearranging the observed R-D signal into a long vector. For the tensor-based scheme, the natural property that the sampled R-D harmonic signal is tensorial data motivates the advent of the tensor-based scheme. Herein, the HOSVD and CPD are two commonly used methods, which are viewed as the generalization of the matrix SVD [10]. For HOSVD, its combination with ESPRIT (also known as Tensor ESPRIT) [27], structure least squares [18], or iteratively reweighted framework [28], [29] are explored to solve the MHR problem. For CPD, its generalized Vandermonde [9], [30] and coupled frameworks [11] are developed for the same purpose.

While the above-discussed studies have achieved significant developments, the accurate estimation of the parameters of the R-D harmonic signal in MIMO models is still an open and challenging problem. The proposed estimator should be able to achieve a small error between the estimated and actual values. Ideally, it should approach the Cramér–Rao lower bound. Additionally, it is desirable to have a low-computational complexity and maintain noise immunity to ensure reliable performance in practical applications [10], [30]. The relevance of such advancements extends beyond the realm of MIMO communication systems, finding applications in emerging technologies, such as the IoT [31]. In MIMO scenarios, where multiple antennas are employed for simultaneous communication, the accurate estimation of harmonic signal parameters is fundamental for optimizing spectral efficiency and enhancing overall system performance [32]. Several methods, including sparse Bayesian learning [33] and spatial basis expansion model [34], have been developed to leverage the structure of MIMO channels to enhance channel estimation and tracking. Additionally, with the increasing integration of wireless communication in IoT devices, the proposed estimator holds promise in addressing the unique challenges posed by the diverse communication environments within the IoT ecosystem [35], [36].

In this work, we propose a tensor-based data-driven approach for MHR in channel sounding based on high-order dynamic mode decomposition (HODMD), which is a tensor-based scheme combining HOSVD and dynamic mode decomposition (DMD). Herein, HOSVD is first applied to decompose the original measured tensorial data, which yields the low-rank core tensor and mode matrices along R dimensions. Then, DMD is employed to represent each mode matrix in terms of dynamic modes and DMD eigenvalues. The resultant DMD eigenvalues of the rth mode matrix imply the parameters of interest along the corresponding dimension. This sub-procedure can be executed in parallel. Finally, all frequencies of interest are estimated, and MHR is obtained. Our contributions can be summarized as follows.

1) We propose a novel tensor-based approach, HODMD, to estimate the frequencies of interest for R-D sinusoids in the presence of additive white Gaussian noise for MIMO wireless channel sounding. The proposed method demonstrates its efficacy in MHR, accommodating both single and multiple tones at single and multiple snapshots.
2) The proposed method incorporates a capability to automatically estimate the number of tones within the undamped multidimensional signal during the decomposition process. This feature is particularly valuable in practical applications where the number of tones may be unknown. The ability to determine the number of tones enhances the adaptability of our method to real-world scenarios, making it a valuable tool in situations where prior knowledge of signal characteristics is limited.
3) The HODMD method leverages truncation operations in HOSVD and DMD to purify processed data. By preserving the signal subspace and discarding the noise subspace, our approach effectively enhances the signal quality. Additionally, the incorporation of moving averages in preparing input data further improves denoising efficiency. Consequently, the proposed HODMD method exhibits superior performance in scenarios with high SNR compared to similar approaches. This noise reduction capability enhances the reliability and accuracy of frequency estimation in practical MIMO wireless communication systems.

The remainder of this article is outlined as follows. Section II comprehensively elucidates the formulation of the MHR problem and underscores its practical application through a specific illustration, namely, the double-directional MIMO channel model. Following this, Section III introduces two pertinent methodologies, namely, SVD and HOSVD. The proposed HODMD approach is explicated in the same section, and its efficacy is substantiated through numerical simulations in Section IV. Finally, the conclusions are presented in Section V.

II. Background

A. Notation

The mathematical notation used in this article can be found in Table I. Herein, the lowercase, bold lowercase, bold uppercase, and bold calligraphy Latin letters are used to denote the scalars (e.g., $a, b, c, \ldots$), vectors (e.g., $\boldsymbol{a}, \boldsymbol{b}, \boldsymbol{c}, \ldots$), matrices (e.g., $\mathbf{A}, \mathbf{B}, \mathbf{C}, \ldots$), and tensor (e.g., $\boldsymbol{\mathcal{A}}, \boldsymbol{\mathcal{B}}, \boldsymbol{\mathcal{C}}, \ldots$), respectively. The transpose, conjugate transpose, complex conjugate, inverse, and pseudoinverse of a matrix is denoted by $(\cdot)^{\mathrm{T}}$, $(\cdot)^{\mathrm{H}}$, $(\cdot)^{*}$, $(\cdot)^{-1}$, and $(\cdot)^{\dagger}$. $\mathcal{A} \in \mathbb{C}^{M_1 \times M_2 \times \cdots \times M_r \times \cdots \times M_R}$ refers to a R-order tensor, whose the $(m_1, m_2, \ldots, m_R)$ entry is denoted as $a_{m_1, m_2, \ldots, m_R}$.

B. Problem Formulation of Multidimensional Harmonic Retrieval

We introduce hereafter the problem formulation of the R-D HR. Assumed that R-D HR signal is sampled for K snapshots

TABLE I
NOTATIONS AND CORRESPONDING DESCRIPTIONS

Notations	Descriptions
$a, b, c, \ldots$	scalars
$\boldsymbol{a}, \boldsymbol{b}, \boldsymbol{c}, \ldots$	vectors
$\boldsymbol{\mathcal{A}}, \boldsymbol{\mathcal{B}}, \boldsymbol{\mathcal{C}}, \ldots$	tensors
$(\cdot)^T$	transpose
$(\cdot)^H$	conjugate transpose
$(\cdot)^*$	complex conjugate
$(\cdot)^{-1}$	inverse
$(\cdot)^\dagger$	pseudoinverse
$\widetilde{(\cdot)}$	low-dimensional matrix in DMD
$\widehat{(\cdot)}$	low-dimensional matrix in HODMD
$\overline{(\cdot)}$	state in moving average
$\check{(\cdot)}$	estimated value
$(\cdot)_s$	signal component
$(\cdot)_n$	noise component
$\mathbb{C}^{M_1 \times M_2 \times \cdots \times M_r \times \cdots \times M_R}$	set of $M_1 \times M_2 \times \cdots \times M_r \times \cdots \times M_R$ complex tensor
$(\cdot)_{m_1, m_2, \ldots, m_R}$	$(m_1, m_2, \ldots, m_R)$ entry of R-order tensor $\boldsymbol{\mathcal{A}} \in \mathbb{C}^{M_1 \times M_2 \times \cdots \times M_r \times \cdots \times M_R}$

with additive noise. Then, the collected tensor data is

$$\boldsymbol{\mathcal{T}} = \boldsymbol{\mathcal{S}} + \boldsymbol{\mathcal{N}}. \tag{1}$$

Herein, $\boldsymbol{\mathcal{S}}$ denotes the signal component, and its entries are formed as [18]

$$s_{k,m_1,m_2,\ldots,m_R} = \sum_{i=1}^{I} \gamma_i(k) \prod_{r=1}^{R} e^{j\omega_{r,i} m_r} \tag{2}$$

where $m_r = 1, 2, \ldots, M_r, r = 1, 2, \ldots, R, k = 1, 2, \ldots, K$, and $i = 1, 2, \ldots, I$. M_r, R, K, and I refer to the number of the rth dimension's sampling points, dimensions, snapshots, and tones. $\gamma_i(k)$ means the complex amplitude of the ith source sampled at the kth snapshot, whose power is denoted as $\mathbb{E}\{|\gamma_i(k)|^2\} = \sigma_i^2$. $\omega_{r,i} \in (-\pi, \pi)$, $r = 1, 2, \ldots, R$, $i = 1, 2, \ldots, I$, corresponds to the R-D frequencies of interest. $\boldsymbol{\mathcal{T}}, \boldsymbol{\mathcal{S}}$, and $\boldsymbol{\mathcal{N}} \in \mathbb{C}^{K \times M_1 \times M_2 \times \cdots \times M_R}$. $\boldsymbol{\mathcal{N}}$ denotes the additive noise component, and its entries are zero mean circularly symmetric complex Gaussian random variables with an identical variance σ_N^2. The task of MHR is to estimate the frequencies, namely, $\omega_{r,i}, r = 1, 2, \ldots, R, i = 1, 2, \ldots, I$, from the collected tensor $\boldsymbol{\mathcal{T}}$. In this scenario, we assumed that $I < M_r, i = 1, 2, \ldots, I$. Notably, (2) corresponds to the undamped case. When the damped sinusoidal model is considered, the exponential term $e^{j\omega_{r,i} m_r}$ becomes $e^{(\rho_{r,i} + j\omega_{r,i}) m_r}$, where $\rho_{r,i}$, $r = 1, 2, \ldots, R$, and $i = 1, 2, \ldots, I$ denotes the R-D damping factors of interest.

C. Double-Directional MIMO Channel Sounding

The double-directional MIMO channel model can be considered a typical MHR problem [2], [3], [37]. Fig. 1 illustrates an environment where the wireless propagation is primarily characterized by three dominant signal paths. The channel considered is a double-directional MIMO channel, utilizing a uniform linear array (ULA) for both the transmitter and receiver. The three dominant signal paths represent the I parameters in (3). And each path is uniquely defined by

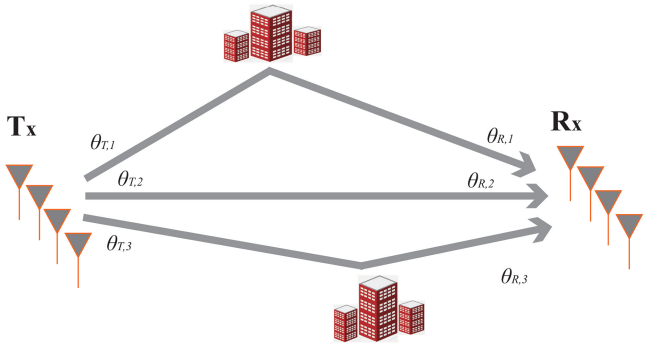

Fig. 1. Illustration of a double-directional MIMO wireless channel with three paths.

parameters, such as the DOD from the transmitter antenna array, the DOA at the receiver antenna array, time-varying complex path loss incorporating Doppler effects, and the time delay associated with that path. Assuming that the channel's time variation is solely attributed to Doppler shift within the measurement interval, and that path parameters, including Doppler frequencies, remain constant within this interval, the time-varying impulse response between transmit antenna element m_T and receive antenna element m_C can be expressed as follows [1], [3]:

$$\mathcal{Q}\left(m_t, m_f, m_C, m_T\right) = \sum_{i=1}^{I} r_i e^{j2\pi\left(\alpha_i m_t + \tau_i m_f + \frac{1}{\lambda} d_C m_C \cos\theta_{C,i} + \frac{1}{\lambda} d_T m_T \cos\theta_{T,i}\right)}. \tag{3}$$

Herein, we consider a total of I paths, each characterized by specific notations: $\theta_{T,i}$ for DOD, $\theta_{C,i}$ for DOA, τ_i for time delay, α_i for Doppler shift frequency, and r_i for complex path loss. And m_t varies from 0 to $M_t - 1$, m_f from 0 to $M_f - 1$, m_C from 0 to $M_C - 1$, and m_T from 0 to $M_T - 1$. Here, d_C and d_T represent the antenna spacing of the receive ULA and the transmit ULA, respectively. Clearly, channel parameter estimation of this double-directional MIMO system is a 4-D high-resolution problem.

III. METHODOLOGY

This section initiates with an exposition on SVD and HOSVD. The presentation commences with the introduction of the traditional DMD as a solution to the 1-D harmonic retrieval problem. Building upon the conceptual extension of SVD to HOSVD, we further generalize DMD from matrices to tensors. The HODMD is introduced and expounded upon as a methodology designed to address the R-dimensional harmonic retrieval problem.

A. Singular Value Decomposition and High-Order Singular Value Decomposition

Before presenting HODMD, we introduce two related decomposition methods: 1) SVD and 2) HOSVD. As a commonly used factorization method, SVD can be applied for any real-valued or complex-valued matrix, which has been widely explored for the 2-D harmonic retrieval problem [15], [16].

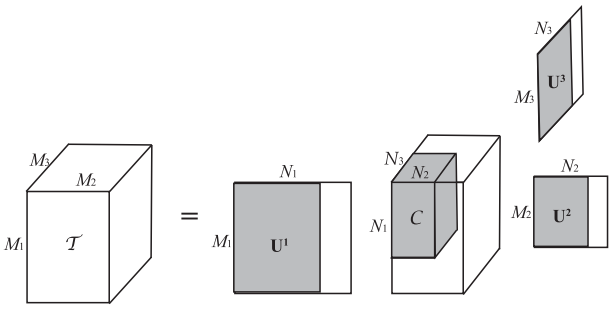

Fig. 2. Illustration of the HOSVD algorithm for a third-order tensor ($R = 3$).

Mathematically, the SVD of a matrix $\mathbf{T} \in \mathbb{C}^{M_1 \times M_2}$ can be expressed as

$$\mathbf{T} = \mathbf{U}\mathbf{S}\mathbf{V}^{\mathrm{H}} \tag{4}$$

where $\mathbf{S}$ is a diagonal matrix with a size of $r \times r$, $\mathbf{U}$ and $\mathbf{V}$ are with the size of $M_1 \times r$ and $M_2 \times r$, whose columns form two sets of orthonormal bases and are denoted as left-singular vectors and right-singular vectors of $\mathbf{T}$, respectively. Notably, when $r < \min\{M_1, M_2\}$, SVD provides a low-rank approximation of matrix $\mathbf{T}$.

When the multidimensional signal is considered, SVD is needed to be modified or extended to deal with the tensor data. To address this non-trivial task, two well-known generalizations has been studied, namely, CPD [9], [11] and HOSVD [17], [18]. Herein, we briefly introduce the latter one. To ease the presentation, we limit ourselves to third-order tensors. Applying the HOSVD of a tensor $\mathcal{T} \in \mathbb{C}^{M_1 \times M_2 \times M_3}$, one can obtain

$$\mathcal{T}_{m_1,m_2,m_3} = \sum_{n_1=1}^{N_1} \sum_{n_2=1}^{N_2} \sum_{n_3=1}^{N_3} \mathcal{C}_{n_1 n_2 n_3} \mathbf{U}^1_{n_1 m_1} \mathbf{U}^2_{n_2 m_2} \mathbf{U}^3_{n_3 m_3} \tag{5}$$

where $N_1, N_2,$ and N_3 refer to the minimal and $N_1 \leq M_1, N_2 \leq M_2,$ and $N_3 \leq M_3$. Tensor $\mathcal{C}$ is the core tensor with dimensions of $N_1 \times N_2 \times N_3$. These minimal values, namely, (N_1, N_2, N_3), denotes the multilinear rank of $\mathcal{T}$. Straightforwardly, $\mathbf{U}^1, \mathbf{U}^2, \mathbf{U}^3$, termed as the mode matrices, are of dimensions of $M_1 \times N_1, M_2 \times N_2, M_3 \times N_3$, respectively. Also, each obtained matrix in HOSVD is unitary, namely, $\mathbf{U}^{1*}\mathbf{U}^1 = \mathbf{I}_{N_1}$, $\mathbf{U}^{2*}\mathbf{U}^2 = \mathbf{I}_{N_2}$, and $\mathbf{U}^{3*}\mathbf{U}^3 = \mathbf{I}_{N_3}$. Fig. 2 plots the illustration of the HOSVD described in (5) for intuitive presentation.

B. Dynamic Mode Decomposition

The DMD approach was first proposed by Schmid and applied in the field of hydrodynamics [38]. It has been demonstrated that this algorithm has a wide application in many areas like orbital angular momentum detection [39], [40], [41], sea clutter modelling [42], global power system [43], etc. To begin with, we consider a 1-D harmonic retrieval with K snapshots to illustrate the procedure of DMD. Following (1) and (2), we have the collected data $\mathbf{T} \in \mathbb{C}^{K \times M_1}$. K means the dimension of each states. To implement DMD, the matrix $\mathbf{T}$ is first split into two adjacent snapshot sequences as

$$\mathbf{T}_1 = [\boldsymbol{t}(\boldsymbol{k}, 1), \boldsymbol{t}(\boldsymbol{k}, 2) \cdots\cdots \boldsymbol{t}(\boldsymbol{k}, M_1 - 1)] \tag{6}$$

$$\mathbf{T}_2 = [\boldsymbol{t}(\boldsymbol{k}, 2), \boldsymbol{t}(\boldsymbol{k}, 2) \cdots\cdots \boldsymbol{t}(\boldsymbol{k}, M_1)] \tag{7}$$

where $\boldsymbol{t}(\boldsymbol{k}, m_1) \in \mathbb{C}^{K \times 1}$ means the m_1th column vector of the matrix $\mathbf{T}$, which refers to the collected harmonic signal at a specific $\boldsymbol{k}$ time. And $\mathbf{T}_1, \mathbf{T}_2 \in \mathbb{C}^{K \times (M_1 - 1)}$. Assumed that two adjacent column, i.e., $\boldsymbol{t}(\boldsymbol{k}, m_1)$ and $\boldsymbol{t}(\boldsymbol{k}, m_1 + 1)$, are related by a linear mapping function $\boldsymbol{F}$, i.e., $\boldsymbol{t}(\boldsymbol{k}, m_1 + 1) = \boldsymbol{F}(\boldsymbol{t}(\boldsymbol{k}, m_1))$. Then, (6) and (7) can be linked by a mapping matrix $\mathbf{A}$, which is given as

$$\mathbf{T_2} = \mathbf{A}\mathbf{T_1}. \tag{8}$$

The DMD algorithm is to calculate the leading eigenvalues and eigenvectors of the mapping matrix $\mathbf{A} \in \mathbb{C}^{K \times K}$. Notably, according to the dynamic theory, the well-known solution of the linear discrete-time system described in (8) is the exponential. Inspired by this, we could derive the frequencies of interest in (2) from the eigenvalues' distribution of $\mathbf{A}$. Herein, we adopt the SVD-based scheme to realize the DMD algorithm [44].

In particular, the SVD algorithm is first adopted for $\mathbf{T_1}$, and one can obtain

$$\mathbf{T_1} = \mathbf{U}\Sigma\mathbf{V}^{\mathrm{H}} = \mathbf{U_s}\Sigma_{\mathbf{s}}\mathbf{V_s^H} + \mathbf{U_n}\Sigma_{\mathbf{n}}\mathbf{V_n^H} \tag{9}$$

where the subscript of s and n stands for signal and noise subspace, respectively. When the number of frequencies I is known in advance, the truncated SVD could be set with the order of I to approximate the signal subspace. Then, substituting (9) into (8), we can construct the mapping matrix $\mathbf{A}$ as

$$\mathbf{A} = \mathbf{T_2}\mathbf{V}\Sigma^{-1}\mathbf{U}^{\mathrm{H}}. \tag{10}$$

Then, the matrix $\mathbf{U_s}$ is utilized to project the original system described in (8) into a low-dimensional system that corresponds to the signal subspace. To be specific, the state in the original system is projected onto the proper orthogonal decomposition (POD) modes, namely, $\widetilde{\mathbf{T_1}} = \mathbf{U}_s^{\mathrm{H}}\mathbf{T}_1$, $\widetilde{\mathbf{T_2}} = \mathbf{U}_s^{\mathrm{H}}\mathbf{T}_2$, and $\widetilde{\mathbf{A}} = \mathbf{U}_s^{\mathrm{H}}\mathbf{A}\mathbf{U}_s$. Combining (8), we have

$$\widetilde{\mathbf{T_2}} = \widetilde{A}\widetilde{T}_1 \tag{11}$$

where $\widetilde{\mathbf{T_1}}, \widetilde{\mathbf{T_2}} \in \mathbb{C}^{I \times (M_1 - 1)}$, and $\widetilde{A} \in \mathbb{C}^{I \times I}$ means the mapping matrix in the low-dimensional system, which captures the governing dynamic behavior in the signal subspace.

Next, the eigenvalue equation for the newly constructed low-dimensional system is analyzed by the eigendecomposition of $\widetilde{A}$, which is expressed as

$$\widetilde{\mathbf{A}}\mathbf{E} = \mathbf{E}\Lambda \tag{12}$$

where $\boldsymbol{E} \in \mathbb{C}^{I \times I}$ refers to a square matrix with an order of I, whose columns denote the eigenvectors. $\Lambda \in \mathbb{C}^{I \times I}$ refers to a diagonal matrix, whose entries correspond to the eigenvalues, namely, $\lambda_i, i = 1, 2 \ldots I$. Based on the decomposed result in (12), we construct the eigenvector of the original system (see Appendix A). Then, we define a matrix that corresponds to the dynamic mode as

$$\mathbf{D} = \mathbf{T_2}\mathbf{V_s}\Sigma_{\mathbf{s}}^{-1}\mathbf{E}. \tag{13}$$

Finally, the 1-D harmonic signal at the m_1th sampling position can be expressed as

$$\boldsymbol{t}(\boldsymbol{k}, m_1) = \sum_{i=1}^{I} b_i \boldsymbol{d}_i e^{\alpha_i m_1} = \sum_{i=1}^{I} b_i \boldsymbol{d}_i e^{(\alpha_i^r + j\alpha_i^i) m_1} \tag{14}$$

where $\boldsymbol{d}_i$ refers to the dynamic mode, which is the ith column of the matrix $\mathbf{D} \in \mathbb{C}^{K \times I}$. b_i denotes the amplitude weight of ith dynamic mode. $\alpha_i = \alpha_i^r + j\alpha_i^i = \ln(\lambda_k)/\Delta m_1$, λ_i means the ith eigenvalue in (12), and Δm_1 means the sampling interval in M_1 dimension. The distribution of α_i is termed the DMD spectrum. It is straightforward that α_i^r and α_i^i correspond to the damping factor and frequency, respectively. Equation (14) is derived from (13) through the eigenvalue decomposition of $\mathbf{A}$, allowing us to represent the evolution of the system in an exponential form. This compact representation leverages the eigenvalues and eigenvectors to describe how each mode evolves, providing a clear and insightful description of the system's dynamics. Hence, through the decomposition shown in (14), the governing equation of the considered harmonic signal is obtained. That is to say, the damping factors and frequencies of interest are derived accordingly.

Moreover, the moving average can be adopted in reorganizing the input data, i.e., $\mathbf{T}_1$ in (6) and $\mathbf{T}_2$ in (7) to enhance the denoising efficacy. Specifically, it involves selecting a fixed number of columns to perform moving average on the input matrix after obtaining the original input data. Detailed derivations are provided in Appendix B. This moving average preserves the mapping relationships in signal space while attenuating component in the noise space. This moving average approach is used here to mitigate the impact of Gaussian white noise interference. Importantly, the utilization of moving average in the DMD framework does not necessitate additional supplementary information. It is worth noting that both the DMD algorithm and its average variation, as the purely data-driven scheme, builds the governing equation merely based on the observed data. Algorithm 1 plots the pseudocode of DMD for dealing with the 1-D harmonic signal. Notably, we assume that the sequence $\mathbf{T_2}$ can be linearly mapped from the sequence $\mathbf{T_1}$ through the matrix $\mathbf{A}$. This assumption forms the basis of DMD, where we seek to find a linear operator that best advances the system from one snapshot in time to the next. Also, to reduce the dimensionality and focus on the most significant dynamic modes, we project the high-dimensional system into a low-dimensional subspace. This projection ensures that $\widetilde{\mathbf{A}}$ captures the dominant dynamics of the system in a reduced space, making the subsequent eigenanalysis computationally efficient while preserving the essential characteristics of the original system.

Algorithm 1: DMD for 1-D Harmonic Retrieval

Input: The observed 1-D harmonic signal: $\mathbf{T}$; The sampling interval: Δm_1; Total number of tones: I
Output: Frequencies: $\omega_{1,i}$
1 Build adjacent snapshot sequences: $\mathbf{T_1}$ and $\mathbf{T_2}$;
2 Linear mapping assumption: $\mathbf{T_2} = \mathbf{A}\mathbf{T_1}$;
3 Construct mapping matrix: $\mathbf{A} = \mathbf{T_2}\mathbf{V}\Sigma^{-1}\mathbf{U}^*$;
4 Project to low-dimensional system: $\widetilde{\mathbf{T_2}} = \widetilde{A}\widetilde{T_1}$;
5 Eigendecomposition: $\widetilde{\mathbf{A}}\mathbf{E} = \mathbf{E}\Lambda$;
6 Define the dynamic mode: $\mathbf{D} = \mathbf{T_2}\mathbf{V_s}\Sigma_{\mathbf{s}}^{-1}\mathbf{E}$;
7 Obtain the governing equation of 1-D harmonic signal;
8 **Return** $\omega_{1,i}$ from the eigenvalue distribution $(\alpha_{1,i})$;

C. High-Order Dynamic Mode Decomposition

When we consider the R-D harmonic retrieval problem, the DMD described earlier that is applied to deal with the matrix cannot be adapted to tensor data. To address this issue, we extend the DMD algorithm to tensor decomposition, namely, HODMD. Herein, a 3-D harmonic retrieval problem is considered for the illustration. We assumed that the harmonic signal is collected at one snapshot, i.e., $K = 1$. Then, a third-order tensor $\mathcal{T} \in \mathbb{C}^{M_1 \times M_2 \times M_3}$ can be obtained through the observation.

Similar to how DMD handles matrices with SVD, HODMD also first deals with the tensor data with HOSVD. One can obtain

$$\mathcal{T}_{m_1,m_2,m_3} = \sum_{i_1=1}^{I}\sum_{i_2=1}^{I}\sum_{i_3=1}^{I} \mathcal{C}_{i_1 i_2 i_3} \mathbf{U}^1_{i_1 m_1} \mathbf{U}^2_{i_2 m_2} \mathbf{U}^3_{i_3 m_3}. \tag{15}$$

Herein, we truncate each dimension to the order of I to correspond to the signal subspace. Through this decomposition, the low-rank core tensor $\mathcal{C} \in \mathbb{C}^{I \times I \times I}$ is obtained. Also, the mode matrices $\mathbf{U}^1$, $\mathbf{U}^2$, and $\mathbf{U}^3$ with size of $I \times M_1$, $I \times M_2$, and $I \times M_3$ are obtained, whose entries are $\mathbf{U}^1_{i_1 m_1}$, $\mathbf{U}^2_{i_2 m_2}$, and $\mathbf{U}^3_{i_3 m_3}$, respectively.

Then, the DMD is used to express these mode matrices in exponential form as shown in (14). In particular, we use the mode matrix in the third dimension, namely, $\mathbf{U}^3$, as an example. For convenience, (15) can be rewritten as follows:

$$\mathcal{T}_{m_1,m_2,m_3} = \sum_{i_1=1}^{I}\sum_{i_2=1}^{I}\sum_{i_3=1}^{I} \widehat{\mathcal{C}}_{i_1 i_2 i_3} \widehat{\mathbf{U}}^3_{i_3 m_3} \tag{16}$$

with

$$\widehat{\mathcal{C}}_{i_1 i_2 i_3} = \frac{1}{\zeta^3_{m_3}} \sum_{i_1=1}^{I}\sum_{i_2=1}^{I} \mathcal{C}_{i_1 i_2 i_3} \mathbf{U}^1_{i_1 m_1} \mathbf{U}^2_{i_2 m_2} \tag{17}$$

and

$$\widehat{\mathbf{U}}^3_{i_3 m_3} = \zeta^3_{m_3} \mathbf{U}^3_{i_3 m_3} \tag{18}$$

where $\widehat{\mathcal{C}}_{i_1 i_2 i_3}$ and $\widehat{\mathbf{U}}^3_{i_3 m_3}$ is the rescaled core tensor and rescaled mode matrix respectively. $\zeta^3_{m_3}$ denotes the third dimension's HOSVD singular values of $\mathcal{T}$. The column of rescaled mode matrix is expressed as

$$\widehat{\mathbf{U}}^3_{i_3 m_3} = \left[\widehat{\mathbf{u}}_{I,1}, \widehat{\mathbf{u}}_{I,2}, \ldots, \widehat{\mathbf{u}}_{I,m_3}, \ldots, \widehat{\mathbf{u}}_{I,M_3}\right] \tag{19}$$

where

$$\widehat{\mathbf{u}}_{I,m_3} = \begin{bmatrix} \widehat{u}_{1,m_3} \\ \widehat{u}_{2,m_3} \\ \cdots \\ \widehat{u}_{I,m_3} \end{bmatrix}. \tag{20}$$

Referring to (14), we process the rescaled mode matrix $\widehat{\mathbf{U}}^3_{i_3 m_3}$ via the DMD algorithm. Then, the column state of this matrix with the index of m_3 can be decomposed as

$$\widehat{\mathbf{u}}_{I,m_3} = \sum_{i=1}^{I} b_{3,i}\boldsymbol{d}_{3,i}e^{\alpha_{3,i}m_3} = \sum_{i=1}^{I} b_{3,i}\boldsymbol{d}_{3,i}e^{\left(\alpha^r_{3,i}+j\alpha^i_{3,i}\right)m_3}. \quad (21)$$

Substituting (21) into (16), we have

$$\mathcal{T}_{m_1,m_2,m_3} = \sum_{i=1}^{I} b_{3,i}\mathcal{D}_{m_1,m_2,i}e^{\left(\alpha^r_{3,i}+j\alpha^i_{3,i}\right)m_3} \quad (22)$$

where

$$\mathcal{D}_{m_1,m_2,i} = \sum_{i=1}^{I} \widehat{\mathcal{C}}_{i_1 i_2 i_3}\boldsymbol{d}_{3,i} \quad (23)$$

where $\mathcal{D}_{m_1,m_2,i}$ is the tensor dynamic mode of third dimension of $\mathcal{T}$. The physical meaning of (22) is straightforward. The observed tensor data is decomposed into I exponential components along the third dimension. Comparing (22) with (2), we can derive the damping factors and frequencies of the third dimension of interest from the distribution of $\alpha^r_{3,i}$ and $\alpha^i_{3,i}$, respectively.

Likewise, we adopt the DMD algorithm to analyze the remaining mode matrices, namely, $\mathbf{U}^1$ and $\mathbf{U}^2$. The damping factors and frequencies of interest along the corresponding dimension can be derived accordingly. It is worth noting that, thanks to the HOSVD, we only need to analyze the mode matrix to obtain the frequency parameters. Compared to the harmonic extraction by reshaping the original tensor to a long vector or matrix, our proposed tensor decomposition approach only needs to deal with obtained matrices with fewer dimensions, namely, each mode matrix, which could greatly improve computational efficiency. While the proposed HODMD method is initially presented for the case of a single snapshot ($K = 1$), it is important to note that $K = 1$ is a special and challenging case in the context of MHR. When $K > 1$, we could perform calculations and average the results across each dimension, ensuring that the harmonic retrieval process is robust and accurate. Therefore, the proposed HODMD method is applicable and effective for cases with $K > 1$. Also, this calculation process is performed separately after HOSVD and can be run in parallel. The pseudocode of HODMD for the R-D harmonic retrieval is given in Algorithm 2. Notably, our proposed HODMD method is fundamentally data-driven, as it builds upon the principles of DMD. DMD is a classic data-driven technique that operates directly on the observed data. This approach does not rely on predefined models, allowing it to adapt to and learn from the underlying data structures and patterns. By integrating HOSVD, DMD, and moving average techniques, our method processes high-dimensional signals, mitigating noise interference and efficiently estimating frequencies of interest. This tensor-based data-driven nature ensures that our method is capable of handling various types of high-dimensional signals without prior assumptions about the data distribution.

Algorithm 2: HODMD for R-D Harmonic Retrieval

Input: The observed R-D harmonic signal: $\mathcal{T}_{m_1,m_2,\ldots,m_R}$;
The sampling interval vector:
$\Delta\boldsymbol{m_r}, r = 1, 2, \ldots, R$; Total number of tones: I

Output: Frequencies: $\omega_{r,i}, r = 1, 2, \ldots, R, i = 1, 2, \ldots, I$

Implement HOSVD on $\mathcal{T}_{m_1,m_2,\ldots,m_R}$;
for $r = 1, \ldots, R$ **do**
  Construct the rescaled mode matrix: $\widehat{\mathbf{U}}^r_{i_r m_r}$;
  Implement DMD for $\widehat{\mathbf{U}}^r_{i_r m_r}$;
  Obtain the rth dimensions' DMD spectrum: $\alpha^r_{r,i} + j\alpha^i_{r,i}$;
  Derive $\omega_{r,i}$ from the eigenvalue distribution $(\alpha_{r,i})$
end
Return R-D signals' frequencies;

IV. Results

We explore several numerical examples to validate the proposed HODMD approach in the following. Specifically, the basic DMD scheme is first benchmarked by a 1-D harmonic retrieval problem. Then, HODMD is verified by a 3-D harmonic retrieval problem. Finally, the performances of the proposed scheme, including the noise and computational complexity analysis, are studied for further validation.

A. 1-D Harmonic Retrieval

To verify DMD, we first consider a 1-D harmonic retrieval example. Herein, the three undamped harmonic signal tones are analyzed with the frequencies of $\omega_{1,1} = 0.2 * 2\pi, \omega_{1,2} = 0.3 * 2\pi, \omega_{1,3} = 0.5 * 2\pi$ in the noise-free environment. Assumed that the temporal components are also exponentially distributed, and the power of each frequency is 1, namely, $\sigma_1^2 = \sigma_2^2 = \sigma_3^2 = 1$. $M_1 = 10$ sampling points with $K = 8$ snapshots are collected. Thus, the formed original input data is $\mathbf{T} \in \mathbb{C}^{8\times 10}$, as shown in Fig. 3(a). We can obtain three dynamic modes by applying DMD to deal with the input data $\mathbf{T}$. Fig. 4 shows the distribution of the corresponding eigenvalues, namely, DMD spectrum α_i in (14). It is clear that the real part of each eigenvalue corresponds to the damping factor, which is all zero. Also, the imaginary part corresponds to the frequency, where the frequency can be derived correctly. Hence, we can conclude that the damping factor and frequency can be derived accurately via the DMD method.

In addition, according to the decomposed expression of harmonic signal in (14), we reconstruct the original input data based on the dynamic modes and corresponding eigenvalues. Fig. 3(b) plots the reconstructed signal, and Fig. 3(c) shows the pixel-by-pixel absolute error distribution between the original signal and the reconstructed one. It is found that the original and reconstructed signals are intuitively consistent, and the error of each pixel is tiny. Hence, the input data is well reconstructed via DMD.

Notably, the previous decomposition is based on the fact that the number of tones is known in a prior. However, in several practical application examples, the number of tones cannot be obtained in advance. Therefore, the estimation of

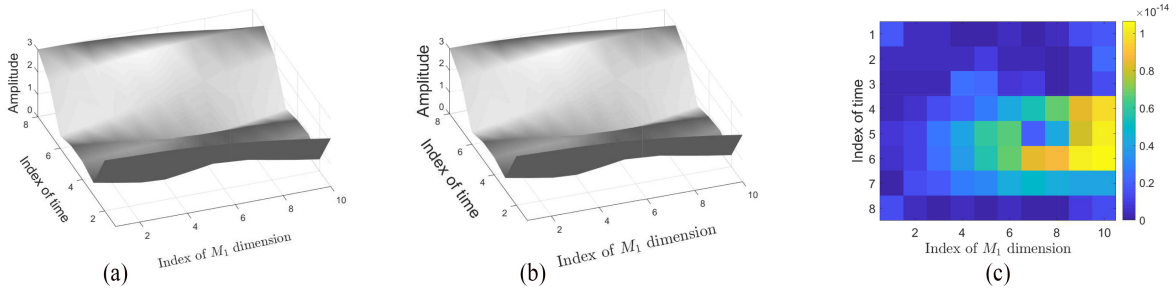

Fig. 3. Visualization of (a) the observed harmonic signal, (b) DMD reconstruction, and (c) error distribution.

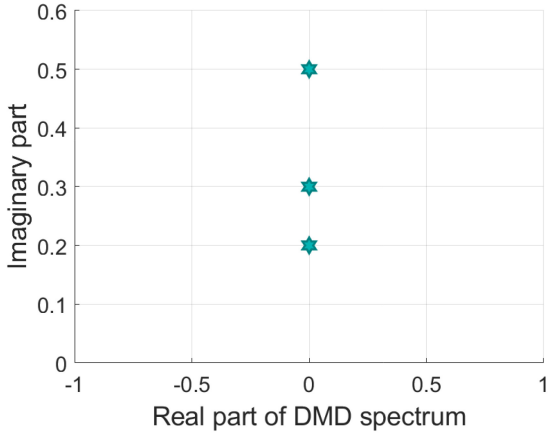

Fig. 4. Distribution of the DMD spectrum.

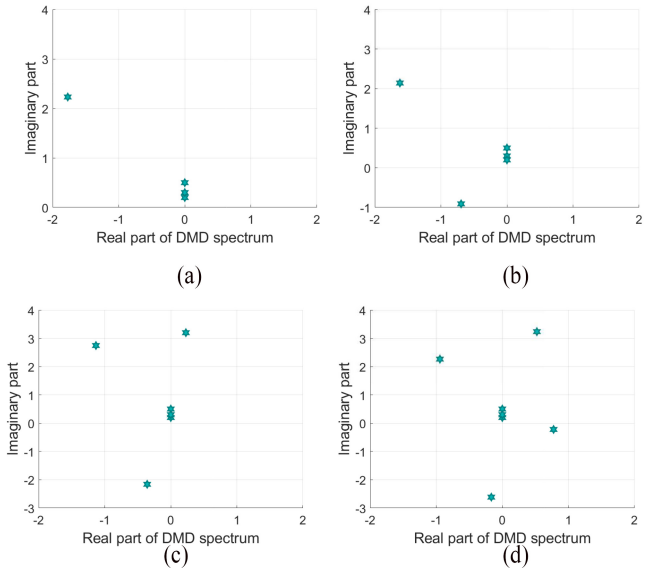

Fig. 5. Distribution of the DMD spectrum with truncation order of (a) 4, (b) 5, (c) 6, and (d) 7 for the unknown tones' number case.

the number of tones is also a challenge in the MHR problem. In our scenario, the number of tones implies the truncation order in the first SVD step. And the damping factors and frequencies are derived from the real and imaginary parts of the eigenvectors. For the undamped case, the real part of all eigenvectors should be zero. This can help assert the number of tones. To be specific, when the number of tones is unknown, we could truncate SVD with a large order, which should be larger than the actual tones' number. The eigenvalues with the real part of zero correspond to the actual tones in the undamped signal. That is to say, the number of tones can be obtained by counting the eigenvalues whose real part is 0, which can be defined as

$$\breve{I} = \sum_{i=1}^{I_{\text{larg}}} \mathbb{1}\left(\alpha_i^r < \varepsilon\right) \tag{24}$$

where $\breve{I}$, I_{larg}, and ε mean the estimated tones' number, the truncation order, and the error threshold. Generally, $I_{\text{larg}} > I$, and ε is set to be a specific small value. Equation (24) means that as long as the real part of the eigenvalue is less than the error threshold, then its imaginary part corresponds to an actual frequency component. As a result, the number of eigenvalues that satisfy this criterion corresponds to the number of tones.

We consider the previous case plotted in Fig. 3 for verification. We set the truncation order I_{larg} to 4, 5, 6, and 7, respectively. Through DMD, the obtained DMD spectrum is shown in Fig. 5. It is clear that, in each case, the number of eigenvalues satisfying the discriminant condition is 3, which is consistent with the actual situation. Hence, the DMD approach can also estimate the number of tones in the 1-D harmonic retrieval process.

B. R-D Harmonic Retrieval

In the following, we demonstrate the HODMD method by analyzing a 3-D example. Two undamped tones are considered, namely, $\omega_{1,1} = 0.1 * 2\pi, \omega_{1,2} = 0.2 * 2\pi, \omega_{1,3} = 0.3 * 2\pi$ for the first tone and $\omega_{2,1} = 0.35 * 2\pi, \omega_{2,2} = 0.25 * 2\pi, \omega_{2,3} = 0.15 * 2\pi$ for the second tone. The other parameters are $M_1 = 14, M_2 = 15, M_3 = 16, K = 1, \sigma_1 = \sigma_2 = 1$. Thus, the task is to estimate 3 frequencies pairs from the collected tensor $\mathcal{T} \in \mathbb{C}^{14\times15\times16}$. Fig. 6 plots the 3-D amplitude distribution of tensor $\mathcal{T}$. HOSVD is first applied to decompose the input tensor. Unlike the SVD with singular values in the matrix decomposition, the core tensor $\mathcal{C}$ obtained in HOSVD is not diagonal. Herein, the Frobenius norms of the corresponding slices obtained by fixing the specific index are used as the HOSVD singular values. As shown in Fig. 7, singular values greater than the index of 2 for each dimension are approximately 0, and thereby the order or rank of each dimension is 2.

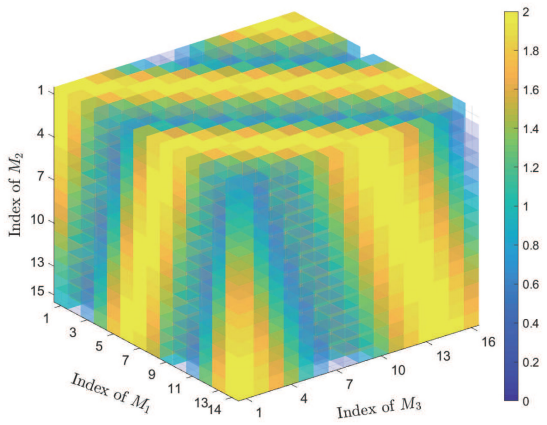

Fig. 6. Visualization of the 3D distribution of amplitude of the collected data $\mathcal{T} \in \mathbb{C}^{14\times15\times16}$ with two undamped tones: $\omega_{1,1} = 0.1 * 2\pi, \omega_{1,2} = 0.2 * 2\pi, \omega_{1,3} = 0.3 * 2\pi$ for the first tone and $\omega_{2,1} = 0.35 * 2\pi, \omega_{2,2} = 0.25 * 2\pi, \omega_{2,3} = 0.15 * 2\pi$ for the second tone.

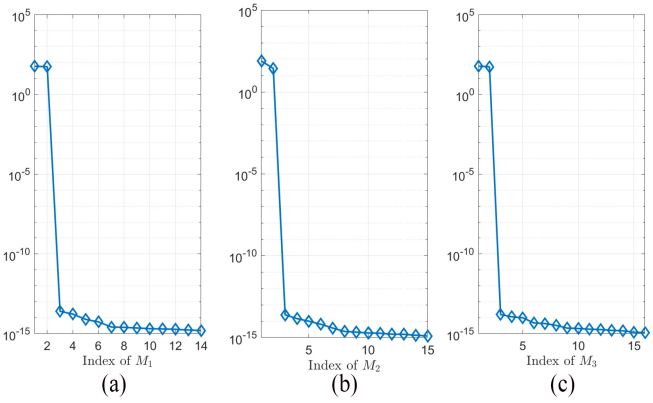

Fig. 7. Distribution of the multilinear singular values by fixing the index at the (a) first, (b) second, and (c) third dimension.

By setting the truncation order for each dimension to 2, we can obtain $\mathcal{C} \in \mathbb{C}^{2\times2\times2}$, $\mathbf{U}^1 \in \mathbb{C}^{2\times14}$, $\mathbf{U}^2 \in \mathbb{C}^{2\times15}$, and $\mathbf{U}^3 \in \mathbb{C}^{2\times16}$, based on (15). Fig. 8(a), (c), and (e) show the amplitude distribution of the obtained mode matrices, namely, $\mathbf{U}^1$, $\mathbf{U}^2$, and $\mathbf{U}^3$, respectively. Then, we use DMD to analyze these mode matrices. The DMD spectrum of these three mode matrices can be obtained, which is plotted in Fig. 8(b), (d), and (f). Take $\mathbf{U}^1$ as an example, whose DMD spectrum is shown in Fig(b), we can see that the imaginary part of the eigenvalues correctly implies the frequencies in the first dimension, i.e., $\omega_{1,1} = 0.1 * 2\pi$ and $\omega_{2,1} = 0.35 * 2\pi$. Also, the frequencies of interest and the imaginary parts of the eigenvalues are consistent in the remaining dimension. Finally, all the frequencies of interest in all three dimensions are estimated, which is shown in Fig. 9. It is clear that the estimated frequencies are consistent with the actual ones. Hence, the proposed HODMD method can accurately estimate the frequencies from the R-D harmonic signal.

C. Parameter Estimation for Double-Directional MIMO Channel

In (3), the estimation of channel parameters for double-directional MIMO involves a 4-D harmonic retrieval problem.

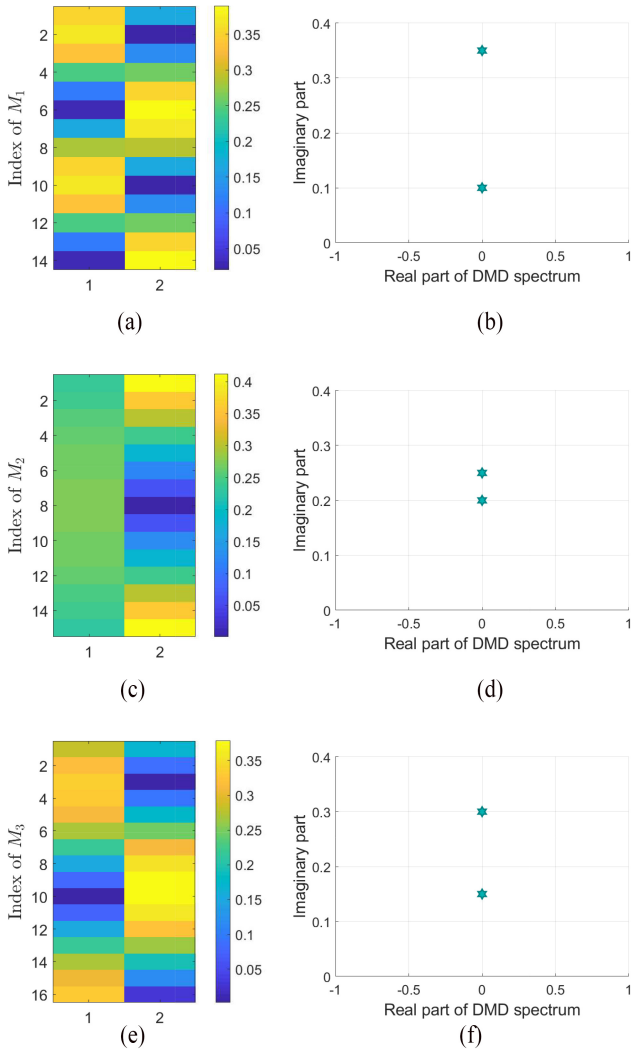

Fig. 8. Amplitude distribution of the mode matrix: (a) $\mathbf{U}^1$, (c) $\mathbf{U}^2$, and (e) $\mathbf{U}^3$. The corresponding DMD spectrum by analyzing (b) $\mathbf{U}^1$, (d) $\mathbf{U}^2$, and (f) $\mathbf{U}^3$.

To simplify this, we reduce the dimensionality to 3 by constraining one dimension. Specifically, when the transmit array lacks harmonic structure, we maintain m_t as a constant, addressing the estimation through a 3-D harmonic retrieval approach. Subsequently, the proposed HODMD method is verified by estimating channel parameters in the double-directional MIMO wireless system. In this numerical example, the double-directional MIMO channel considers three paths with the following parameters: for the first path, $\tau_1 = 0.2$ us, $\theta_{R,1} = 65°$, and $\theta_{T,1} = 50°$; for the second path, $\tau_2 = 0.25$ us, $\theta_{R,2} = 55°$, and $\theta_{T,2} = 40°$; and for the third path, $\tau_3 = 0.3$ us, $\theta_{R,3} = 45°$, and $\theta_{T,3} = 30°$. Other parameters are $M_f = 10$, $M_R = 9$, $M_T = 8$, and the SNR is set to 10 dB in the example.

The proposed HODMD method is then employed to obtain the parameters for each path, as depicted in Fig. 10(a). Table II presents a comparison between actual and estimated parameters, revealing a high agreement across all paths. These levels of error are acceptable from an engineering perspective. Additionally, we visualize the DOD versus DOA in Fig. 10(b),

TABLE II
COMPARISON OF ORIGINAL PARAMETERS IN THE DOUBLE-DIRECTIONAL MIMO CHANNEL AND THE ESTIMATED PARAMETERS BY HODMD

Original parameter in double-directional MIMO	estimated parameters by HODMD	Relative error
$(\tau_1 = 0.2$ us, $\theta_{R,1} = 65°$, $\theta_{T,1} = 50°)$	$(\breve{\tau}_1 = 0.2052$ us, $\breve{\theta}_{R,1} = 65.74°$, $\breve{\theta}_{T,1} = 49.26°)$	(2.6% 1.14% 1.48%)
$(\tau_2 = 0.25$ us, $\theta_{R,2} = 55°$, $\theta_{T,2} = 40°)$	$(\breve{\tau}_2 = 0.2537$ us, $\breve{\theta}_{R,2} = 54.32°$, $\breve{\theta}_{T,2} = 40.65°)$	(1.48% 1.24% 1.62%)
$(\tau_3 = 0.3$ us, $\theta_{R,3} = 45°$, $\theta_{T,3} = 30°)$	$(\breve{\tau}_3 = 0.3073$ us, $\breve{\theta}_{R,3} = 44.62°$, $\breve{\theta}_{T,3} = 30.37°)$	(2.43% 0.84% 1.23%)

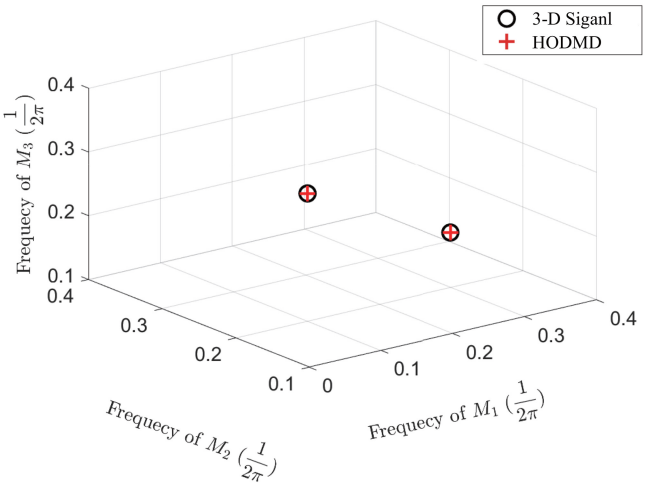

Fig. 9. Comparison between the actual frequencies and these estimated by HODMD with two tones plotted in Fig. 6.

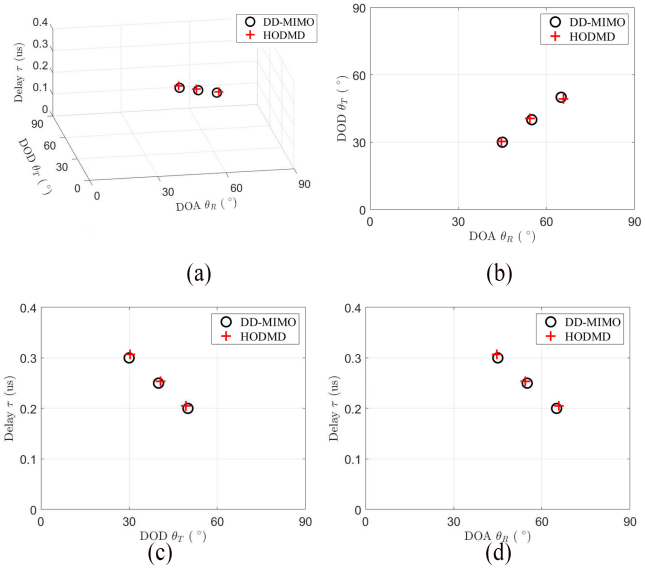

Fig. 10. Results of HODMD applied to parameters' estimation for doubledirectional MIMO wireless system (a) 3-dimension result, (b) DOD and DOA, (c) Delay and DOD, and (d) Delay and DOA: The parameters are: $\tau_1 = 0.2$ us, $\theta_{R,1} = 65°$, and $\theta_{T,1} = 50°$ for the first path; $\tau_2 = 0.25$ us, $\theta_{R,2} = 55°$, and $\theta_{T,2} = 40°$ for the second path; and $\tau_3 = 0.3$ us, $\theta_{R,3} = 45°$, and $\theta_{T,3} = 30°$ for the third path.

DOD versus delay in Fig. 10(c), and DOA versus delay in Fig. 10(d). Evidently, each estimated parameter aligns closely with its true value for every path. Consequently, we can affirm that our proposed RPDMD, as a data-driven method, effectively estimates parameters in the double-directional MIMO channel.

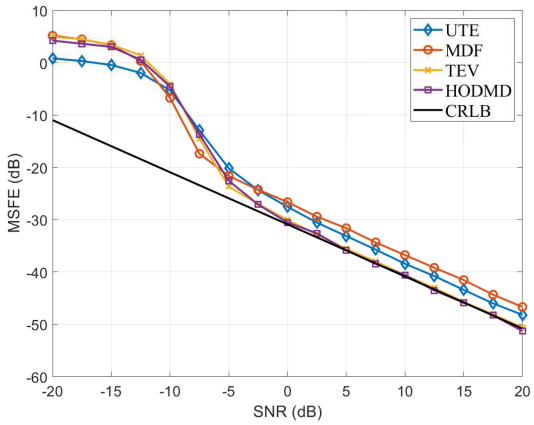

Fig. 11. Average MSFE versus SNR with a single tone.

D. Performance—Noise and Computational Complexity Analysis

Next, we conduct several numerical experiments to further demonstrate the performance of the proposed method. Herein, several similar previous methods are also considered for comparison, including multidimensional folding (MDF) [45], unitary ESPRIT (UE) [24], unitary tensor ESPRIT (UTE) [27], tensor principal-singular-vector utilization for modal analysis (TPUMA) [46], and tensor-eigenvector method (TEV) [18]. Herein, MDF leverages the multidimensional structure of data to improve the efficiency and accuracy of MHR. UE utilizes unitary transformations to exploit Hermitian symmetry, offering efficient computations and improved performance in MHR. UTE extends UE by applying it to tensor data, leveraging the multidimensional nature of the data. TPUMA uses tensor decomposition to extract principal singular vectors for modal analysis. Also, TEV applies eigenvector decomposition to tensor data for parameter estimation in MHR. The close-form CRLB for R-D HR is calculated as a benchmark in each example [47].

The first example is the 3-D HR for the signal with a single tone. The simulation parameters are $\omega_{1,1} = 0.05\pi, \omega_{2,1} = 0.1\pi, \omega_{3,1} = 0.15\pi, I = 1, K = 1, \sigma_1^2 = 1, M_1 = M_2 = M_3 = 6$. We conduct 1000 Monte Carlo runs for each method. And the average mean square frequency error (MSFE) is calculated to measure the performance. The SNR is set from -20 to 20 dB in the interval of 2.5. Fig. 11 shows the comparison result of average MSFE versus SNR. It is clear that when the SNR is greater than -5 dB, TEV and HODMD outperforms other approaches, and they can both reach the value of CRLB when the SNR is greater than 0 dB. When the noise level is high, i.e., SNR < -10 dB, UTE obtains the best

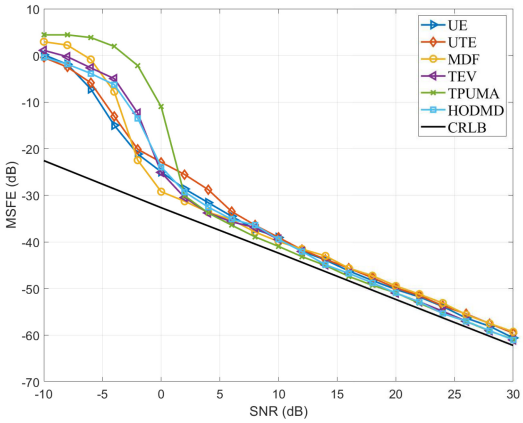

Fig. 12. Average MSFE versus SNR with two tones.

performance. In such high-noise conditions, the performance of the proposed HODMD is similar with the TEV and MDF. Hence, we can conclude that HODMD can be applied for MHR with a single tone at one snapshot. And it can attain the CRLB value in high-SNR situations.

Secondly, we examine a 3-D Harmonic Retrieval scenario featuring two tones. The simulation parameters include $\omega_{1,1} = 0.1\pi, \omega_{2,1} = 0.8\pi, \omega_{3,1} = 0.2\pi, \omega_{1,2} = 0.04\pi, \omega_{2,2} = 0.86\pi, \omega_{3,2} = 0.5\pi, I = 2, K = 1, \sigma_1^2 = \sigma_2^2 = 1, M_1 = M_2 = M_3 = 8$. Similarly, 1000 independent Monte Carlo runs are implemented, and average MSFE is adopted. The SNR is from -10 to 30 dB. Fig. 12 plots MSFE versus SNR. It is observed that the performance of HODMD surpasses that of other approaches for SNR values exceeding 14 dB, demonstrating a superiority margin of approximately 2 dB beyond the CRLB.

Notably, no single method is optimal across all SNR conditions. While our method demonstrates optimal performance at high and low-noise levels due to the integration of moving average and DMD techniques, it does not always outperform others in all SNR scenarios. For instance, although both TPUMA and HODMD achieve optimal performance at SNR values greater than 2 dB, TPUMA's performance deteriorates significantly at SNR values below 2 dB, whereas HODMD maintains a consistent performance. This indicates that our method is a reliable choice across varying SNR levels. Thanks to the integration of HOSVD, DMD, and moving average technology within the HODMD methodology, these contributes to noise interference alleviation, thereby enhancing the accuracy of the mapping matrix decomposition. Consequently, it is evident that HODMD excels in high-SNR situations when addressing the challenge of accurately estimating frequencies in a 3-D signal with two tones. We acknowledge that the improvement is not substantial across all conditions, but we hope to achieve greater advancements through further noise control and optimization in future work.

Finally, we study the computational complexity of the proposed HODMD for further verification. Specifically, the first computational load is from the HOSVD step, which includes $(R+1)$ SVD processes. The corresponding

TABLE III
COMPARISON OF COMPUTATIONAL COMPLEXITY

Method	Computational Complexity
MDF	$\mathcal{O}\left(2IKM^1M^2\right)$, $M^1 = \prod_{r=1}^{R} M_r^1$ $M^2 = \prod_{r=1}^{R} M_r^2$, $M_r^1 + M_r^2 = M_r + 1$
UE	$\mathcal{O}\left(2IK\prod_{r=1}^{R} M_r\right)$
UTE	$\mathcal{O}\left(2IK(R+1)\prod_{r=1}^{R} M_r\right)$
TPUMA	$\mathcal{O}\left((I+1)K\sum_{r=1}^{R} M_r^3\right)$
TEV	$\mathcal{O}\left(I(R+1)K\prod_{r=1}^{R} M_r + \sum_{r=1}^{R} M_r^3 + I\prod_{r=1}^{R} M_r\right)$
HODMD	$\mathcal{O}\left(I(R+1)K\prod_{r=1}^{R} M_r + I\sum_{r=1}^{R} M_r^2 + RI^3\right)$

computational complexity is $\mathcal{O}(I(R+1)K\prod_{r=1}^{R} M_r)$ [48]. The next step is to analyze each decomposed mode matrix via DMD. Take the first mode matrix, i.e., $\mathbf{U}^1 \in \mathbb{C}^{I\times M_1}$, the computational complexity of DMD comes from 2 parts, namely, truncated SVD and eigendecomposition of mapping matrix in the low-dimensional harmonic system. The first part is of $\mathcal{O}(IM_1^2)$, and the second part is of $\mathcal{O}(I^3)$. Thus, the computational complexity of analyzing R mode matrices is $\mathcal{O}(\sum_{r=1}^{R}(IM_r^2 + I^3)) = \mathcal{O}(I\sum_{r=1}^{R} M_r^2 + RI^3)$. Combining the above result. we can derive that the total computational complexity of HODMD is $\mathcal{O}(I(R+1)K\prod_{r=1}^{R} M_r + I\sum_{r=1}^{R} M_r^2 + RI^3)$. For comparison, the computational complexity of other methods used is given in Table III. M_r^1 and M_r^2 are decomposed positive integers such that $M_r^1 + M_r^2 = M_r + 1$. It can be seen that although the computational complexity of the proposed HODMD is similar to the TEV method, both of which adopt HOSVD, HODMD is still better than the TEV method when the sampling number along the dimension is greater than the number of tones, namely, $M_r > I$.

Recent works, such as [49] and [50], have successfully implemented CANDECOMP/PARAFAC decomposition (CPD) models for MIMO channel estimation. CPD-based methods provide low-rank approximations of tensors, which simplifies the model with a combination of vectors. They have been proven effective in channel estimation scenarios. However, CPD and HOSVD primarily focus on dimensionality reduction and may not capture temporal dynamics as effectively [49], [50], [51], [52]. The proposed HODMD method, which integrates HOSVD and DMD, not only offers low-rank representation but also excels in extracting governing equations based on exponential functions from the data. This capability is attributed to the application of DMD to model the matrices derived from HOSVD decompositions. Additionally, since CPD is composed of a set of vectors, integrating CPD with DMD may require an augmented approach to DMD [40], which allows for the effective combination of these methods and could be studied in the future. Notably, our model's adoption of a positive sign in the time delay parameter is consistent with established conventions, as documented in [49], [50], [51]. This choice does not modify the fundamental aspects of signal propagation delay modeling. Additionally, the proposed method can be used for Doppler parameter estimation because the added dimension is an exponential dimension with respect to time, so HODMD can build a model for this 4D signal and estimate parameters.

V. Conclusion

To sum up, we presented a novel approach, HODMD, to solve the MHR problem in MIMO wireless channel sounding. The HODMD method employed a tensor-based analysis approach that first decomposed the observed R-D harmonic signal into a core tensor and mode matrices using HOSVD. Then, DMD was used to process each mode matrix by yielding the DMD spectrum and dynamic modes. Finally, the frequencies of interest were derived from the resultant DMD spectrum distribution. Several numerical experiments were conducted to validate the proposed HODMD method, which was shown to accurately estimate the frequencies of interest from multidimensional signals with single/multiple tones at single/multiple snapshots, determine the number of tones for undamped cases, and provide superior performance in high-SNR situations. Consequently, the HODMD method presented in this work provides a practical and effective tensor-based data-driven solution for the MHR problem.

Appendix A
Construction of Dynamic Mode

The objective of the construction of dynamic mode [definition of the matrix $\mathbf{D}$ in (13)] is to connect the projected low-dimensional system to the original harmonic signal system. Specifically, since $\mathbf{A} = \mathbf{T_2}\mathbf{V}\Sigma^{-1}\mathbf{U}^*$ and $\widetilde{\mathbf{A}} = \mathbf{U_s^*}\mathbf{A}\mathbf{U_s}$, we have

$$\widetilde{\mathbf{A}} = \mathbf{U_s^*}\mathbf{T_2}\mathbf{V}\Sigma^{-1}\mathbf{U}^*\mathbf{U_s}. \tag{25}$$

The noise subspace's term, namely, $\mathbf{U_n^*}$, in the matrix $\mathbf{U}^*$ can be discarded, in which the order of truncation is determined by preserving the larger value of the diagonal elements in Σ. Then, the matrix $\widetilde{\mathbf{A}}$ can be approximated by

$$\widetilde{\mathbf{A}} \approx \mathbf{U_s^*}\mathbf{T_2}\mathbf{V}\Sigma^{-1}. \tag{26}$$

Substituting (26) into (12), we have

$$\mathbf{U_s^*}\mathbf{T_2}\mathbf{V}\Sigma^{-1}\mathbf{E} = \mathbf{E}\Lambda. \tag{27}$$

Premultiplying the preceding equation by $\mathbf{T_2}\mathbf{V}\Sigma^{-1}$, one can obtain

$$\mathbf{T_2}\mathbf{V}\Sigma^{-1}\mathbf{U_s^*}\mathbf{T_2}\mathbf{V}\Sigma^{-1}\mathbf{E} = \mathbf{T_2}\mathbf{V}\Sigma^{-1}\mathbf{E}\Lambda. \tag{28}$$

Since we have $\mathbf{A} = \mathbf{T_2}\mathbf{V}\Sigma^{-1}\mathbf{U}^*$ [see (10)], if we discard the noise subspace's term again and define $\mathbf{D} = \mathbf{T_2}\mathbf{V_s}\Sigma_\mathbf{s}^{-1}\mathbf{E}$, then (28) can be reexpressed as

$$\mathbf{A}\mathbf{D} = \mathbf{D}\Lambda. \tag{29}$$

Hence, the eigendecomposition of the mapping matrix $\mathbf{A}$ is obtained, and the eigenvalue equation of the original harmonic signal system is derived. Notably, it can be seen that the eigenvalues of the constructed low-dimensional system are the same as the original harmonic signal system. The eigenvectors of these two systems are linked by the construction of dynamic modes.

Appendix B
Moving Average of Adjacent Snapshot Sequences

Incorporating moving average technology into DMD proves effective in mitigating the interference of disruptive noise on the computation of the mapping matrix. As previously discussed, the core of the DMD-based method revolves around calculating the leading eigenvalues and eigenvectors of the mapping matrix denoted as $\mathbf{A}$ in $\mathbf{T_2} = \mathbf{A}\mathbf{T_1}$. This computation is grounded on the assumption that two adjacent columns, namely, $\boldsymbol{t}(\boldsymbol{k}, m_1)$ and $\boldsymbol{t}(\boldsymbol{k}, m_1 + 1)$, are linked by a linear mapping function $\boldsymbol{F}$, i.e., $\boldsymbol{t}(\boldsymbol{k}, m_1 + 1) = \boldsymbol{F}(\boldsymbol{t}(\boldsymbol{k}, m_1))$.

Originally expressed as

$$\bar{\bar{\boldsymbol{t}}}_{m_1+1} = \overline{\overline{\boldsymbol{A}}} \cdot \bar{\bar{\boldsymbol{t}}}_{m_1} \tag{30}$$

where $\overline{\overline{(\cdot)}}$ denotes the states in the moving average process. The subsequent summation can be articulated as

$$\sum_{m_1=1}^{P} \bar{\bar{\boldsymbol{t}}}_{m_1+1} = \overline{\overline{\boldsymbol{A}}} \cdot \sum_{m_1=1}^{P} \bar{\bar{\boldsymbol{t}}}_{m_1}. \tag{31}$$

Here, P represents the control parameter for noise averaging. Clearly, if the linear approximation holds for individual terms, i.e., (30), it also holds for their summation, i.e., (31). Given that $\bar{\bar{\boldsymbol{t}}}_{m_1} = \bar{\bar{\boldsymbol{t}}}^{s}_{m_1} + \bar{\bar{\boldsymbol{t}}}^{n}_{m_1}$, the summation can be decomposed into signal and noise components

$$\sum_{m_1=1}^{P} \bar{\bar{\boldsymbol{t}}}_{m_1} = \sum_{m_1=1}^{P} \bar{\bar{\boldsymbol{t}}}^{s}_{m_1} + \sum_{m_1=1}^{P} \bar{\bar{\boldsymbol{t}}}^{n}_{m_1}. \tag{32}$$

Notably, control over P is crucial to ensuring that the data from the 1th to Pth points are spaced less than $1/4$ of the period. Empirically, P could be chosen to include 5-10 adjacent states. This range is generally effective in balancing the trade-off between noise reduction and maintaining the fidelity of the underlying signal. Additionally, this approach maintains the integrity of the signal space by effectively weakening the noise component, considering the mean of Gaussian noise is zero.

References

[1] A. Gershman and N. Sidiropoulos, Eds., *Space-Time Processing for MIMO Communications*. Hoboken, NJ, USA: Wiley, 2005.

[2] C. Qian, X. Fu, N. D. Sidiropoulos, and Y. Yang, "Tensor-based channel estimation for dual-polarized massive MIMO systems," *IEEE Trans. Signal Process.*, vol. 66, no. 24, pp. 6390–6403, Dec. 2018.

[3] M. Steinbauer, A. F. Molisch, and E. Bonek, "The double-directional radio channel," *IEEE Antennas Propag. Mag.*, vol. 43, no. 4, pp. 51–63, Aug. 2001.

[4] K. N. Mokios, N. D. Sidiropoulos, M. Pesavento, and C. Mecklenbrauker, "On 3D harmonic retrieval for wireless channel sounding," in *Proc. IEEE Int. Conf. Acoust., Speech, Signal Process.*, vol. 2, 2004, p. 89.

[5] J. Cong, X. Wang, C. Yan, L. T. Yang, M. Dong, and K. Ota, "CRB weighted source localization method based on deep neural networks in multi-UAV network," *IEEE Internet Things J.*, vol. 10, no. 7, pp. 5747–5759, Apr. 2023.

[6] C. Cheong, Y. Song, Y. Cao, Y. Zhang, B. Cai, and Q. Ni, "Multidimensional trust evidence fusion and path-backtracking mechanism for trust management in VANETs," *IEEE Internet Things J.*, vol. 11, no. 10, pp. 18619–18634, May 2024.

[7] Y. Wang et al., "A multidimensional parallel convolutional connected network based on multisource and multimodal sensor data for human activity recognition," *IEEE Internet Things J.*, vol. 10, no. 16, pp. 14873–14885, Aug. 2023.

[8] P. R. Gomes, J. P. C. da Costa, A. L. de Almeida, and R. T. de Sousa Jr., "Tensor-based multiple denoising via successive spatial smoothing, low-rank approximation and reconstruction for RD sensor array processing," *Digit. Signal Process.*, vol. 89, pp. 1–7, Jun. 2019.

[9] M. Sørensen and L. De Lathauwer, "Multidimensional harmonic retrieval via coupled canonical polyadic decomposition—Part I: Model and identifiability," *IEEE Trans. Signal Process.*, vol. 65, no. 2, pp. 517–527, Jan. 2017.

[10] S. Miron et al., "Tensor methods for multisensor signal processing," *IET Signal Process.*, vol. 14, no. 10, pp. 693–709, 2020.

[11] M. Sørensen and L. De Lathauwer, "Multidimensional harmonic retrieval via coupled canonical polyadic decomposition—Part II: Algorithm and multirate sampling," *IEEE Trans. Signal Process.*, vol. 65, no. 2, pp. 528–539, Jan. 2017.

[12] C. Dai et al., "Video scene segmentation using tensor-train faster-RCNN for multimedia IoT systems," *IEEE Internet Things J.*, vol. 8, no. 12, pp. 9697–9705, Jun. 2021.

[13] Y. Zniyed, R. Boyer, A. L. de Almeida, and G. Favier, "Multidimensional harmonic retrieval based on Vandermonde tensor train," *Signal Process.*, vol. 163, pp. 75–86, Oct. 2019.

[14] X. Nie, L. T. Yang, J. Feng, and S. Zhang, "Differentially private tensor train decomposition in edge-cloud computing for SDN-based Internet of Things," *IEEE Internet Things J.*, vol. 7, no. 7, pp. 5695–5705, Jul. 2020.

[15] S.-Y. Kung, K. S. Arun, and D. B. Rao, "State-space and singular-value decomposition-based approximation methods for the harmonic retrieval problem," *J. Opt. Soc. Am.*, vol. 73, no. 12, pp. 1799–1811, 1983.

[16] S. Bakamidis, M. Dendrinos, and G. Carayannis, "SVD analysis by synthesis of harmonic signals," *IEEE Trans. Signal Process.*, vol. 39, no. 2, pp. 472–477, Feb. 1991.

[17] L. De Lathauwer, B. De Moor, and J. Vandewalle, "A multilinear singular value decomposition," *SIAM J. Matrix Anal. Appl.*, vol. 21, no. 4, pp. 1253–1278, 2000.

[18] W. Sun, H. C. So, F. K. W. Chan, and L. Huang, "Tensor approach for eigenvector-based multi-dimensional harmonic retrieval," *IEEE Trans. Signal Process.*, vol. 61, no. 13, pp. 3378–3388, Jul. 2014.

[19] R. Roy, A. Paulraj, and T. Kailath, "ESPRIT–A subspace rotation approach to estimation of parameters of cisoids in noise," *IEEE Trans. Acoust. Speech Signal Process.*, vol. 34, no. 5, pp. 1340–1342, Oct. 1986.

[20] R. Schmidt, "Multiple emitter location and signal parameter estimation," *IEEE Trans. Antennas Propag.*, vol. 34, no. 3, pp. 276–280, Mar. 1986.

[21] C. Hou, G. Liu, Q. Tian, Z. Zhou, L. Hua, and Y. Lin, "Multisignal modulation classification using sliding window detection and complex convolutional network in frequency domain," *IEEE Internet Things J.*, vol. 9, no. 19, pp. 19438–19449, Oct. 2022.

[22] M. Zoltowski, M. Haardt, and C. Mathews, "Closed-form 2-D angle estimation with rectangular arrays in element space or beamspace via unitary ESPRIT," *IEEE Trans. Signal Process.*, vol. 44, no. 2, pp. 316–328, Feb. 1996.

[23] M. Haardt and J. Nossek, "3-D unitary ESPRIT for joint 2-D angle and carrier estimation," in *Proc. IEEE Int. Conf. Acoust., Speech, Signal Process.*, 1997, pp. 255–258.

[24] M. Haardt and J. Nossek, "Simultaneous Schur decomposition of several nonsymmetric matrices to achieve automatic pairing in multidimensional harmonic retrieval problems," *IEEE Trans. Signal Process.*, vol. 46, no. 1, pp. 161–169, Jan. 1998.

[25] R. Boyer, "Decoupled root-MUSIC algorithm for multidimensional harmonic retrieval," in *Proc. IEEE 9th Workshop Signal Process. Adv. Wireless Commun.*, 2008, pp. 16–20.

[26] X. Qu, Y. Lou, Y. Zhao, Y. Lu, and G. Qiao, "Augmented tensor MUSIC for DOA estimation using nested acoustic vector-sensor array," *IEEE Signal Process. Lett.*, vol. 29, pp. 1624–1628, Jul. 2022.

[27] M. Haardt, F. Roemer, and G. Del Galdo, "Higher-order SVD-based subspace estimation to improve the parameter estimation accuracy in multidimensional harmonic retrieval problems," *IEEE Trans. Signal Process.*, vol. 56, no. 7, pp. 3198–3213, Jul. 2008.

[28] F. Wen and H. C. So, "Robust multi-dimensional harmonic retrieval using iteratively reweighted HOSVD," *IEEE Signal Process. Lett.*, vol. 22, no. 12, pp. 2464–2468, Dec. 2015.

[29] W. Sun, X. Lin, H. C. So, L. Huang, and Q. Li, "Iteratively reweighted tensor SVD for robust multi-dimensional harmonic retrieval," in *Proc. IEEE Int. Conf. Acoust., Speech Signal Process.*, 2016, pp. 4318–4322.

[30] J. M. Papy, L. De Lathauwer, and S. Van Huffel, "Exponential data fitting using multilinear algebra: The single-channel and multi-channel case," *Numer. Linear Algebra Appl.*, vol. 12, no. 8, pp. 809–826, 2005.

[31] A.-S. Bana et al., "Massive MIMO for Internet of Things (IoT) connectivity," *Phys. Commun.*, vol. 37, Dec. 2019, Art. no. 100859.

[32] P. Liu and T. Jiang, "Channel estimation performance analysis of massive MIMO IoT systems with Ricean fading," *IEEE Internet Things J.*, vol. 8, no. 7, pp. 6114–6126, Apr. 2021.

[33] J. Ma, S. Zhang, H. Li, F. Gao, and S. Jin, "Sparse Bayesian learning for the time-varying massive MIMO channels: Acquisition and tracking," *IEEE Trans. Commun.*, vol. 67, no. 3, pp. 1925–1938, Mar. 2019.

[34] H. Xie, F. Gao, S. Zhang, and S. Jin, "A unified transmission strategy for TDD/FDD massive MIMO systems with spatial basis expansion model," *IEEE Trans. Veh. Technol.*, vol. 66, no. 4, pp. 3170–3184, Apr. 2017.

[35] W. Xu et al., "Internet of Vehicles in big data era," *IEEE/CAA J. Automatica Sinica*, vol. 5, no. 1, pp. 19–35, Jan. 2018.

[36] H. Zhou, W. Xu, J. Chen, and W. Wang, "Evolutionary V2X technologies toward the Internet of Vehicles: Challenges and opportunities," *Proc. IEEE*, vol. 108, no. 2, pp. 308–323, Feb. 2020.

[37] R. Parra-Michel, A. Sanchez-Hernandez, C. Salas-Mier, A. Alcocer-Ochoa, and R. Carrasco-Alvarez, "Proper power azimuth spectrum estimation for MIMO channels via GANs mapping inversion," *IEEE Trans. Veh. Technol.*, vol. 71, no. 9, pp. 9143–9158, Sep. 2022.

[38] P. J. Schmid, "Dynamic mode decomposition of numerical and experimental data," *J. Fluid Mech.*, vol. 656, pp. 5–28, Jul. 2010.

[39] Y. Zhang, M. L. Chen, and L. Jiang, "Extraction of the characteristics of vortex beams with a partial receiving aperture at arbitrary locations," *J. Opt.*, vol. 23, no. 8, 2021, Art. no. 085601.

[40] Y. Zhang and L. Jiang, "A novel demultiplexing scheme for vortex beams in radio communication systems," *IEEE Trans. Veh. Technol.*, vol. 70, no. 7, pp. 7243–7248, Jul. 2021.

[41] Y. Zhang, M. L. Chen, and L. Jiang, "Analysis of electromagnetic vortex beams using modified dynamic mode decomposition in spatial angular domain," *Opt. Exp.*, vol. 27, no. 20, pp. 27702–27711, 2019.

[42] Y. Zhang, L. Jiang, and H. T. Ewe, "A novel data-driven modeling method for the spatial-temporal correlated complex sea clutter," *IEEE Trans. Geosci. Remote Sens.*, vol. 60, 2022, Art. no. 5104211.

[43] E. Barocio, B. C. Pal, N. F. Thornhill, and A. R. Messina, "A dynamic mode decomposition framework for global power system oscillation analysis," *IEEE Trans. Power Syst.*, vol. 30, no. 6, pp. 2902–2912, Nov. 2015.

[44] J. N. Kutz, S. L. Brunton, B. W. Brunton, and J. L. Proctor, *Dynamic Mode Decomposition: Data-Driven Modeling of Complex Systems*. Philadelphia, PA, USA: SIAM, 2016.

[45] X. Liu and N. Sidiropoulos, "Almost sure identifiability of constant modulus multidimensional harmonic retrieval," *IEEE Trans. Signal Process.*, vol. 50, no. 9, pp. 2366–2368, Sep. 2002.

[46] W. Sun and H.-C. So, "Accurate and computationally efficient tensor-based subspace approach for multidimensional harmonic retrieval," *IEEE Trans. Signal Process.*, vol. 60, no. 10, pp. 5077–5088, Oct. 2012.

[47] R. Boyer, "Deterministic asymptotic Cramér–Rao bound for the multidimensional harmonic model," *Signal Process.*, vol. 88, no. 12, pp. 2869–2877, 2008.

[48] G. H. Gloub and C. F. Van Loan, *Matrix Computations*, 3rd ed. Baltimore, MD, USA: Johns Hopkins Univ. Press, 1996.

[49] Z. Zhou, J. Fang, L. Yang, H. Li, Z. Chen, and R. S. Blum, "Low-rank tensor decomposition-aided channel estimation for millimeter wave MIMO-OFDM systems," *IEEE J. Sel. Areas Commun.*, vol. 35, no. 7, pp. 1524–1538, Jul. 2017.

[50] R. Zhang et al., "Integrated sensing and communication with massive MIMO: A unified tensor approach for channel and target parameter estimation," *IEEE Trans. Wireless Commun.*, vol. 23, no. 8, pp. 8571–8587, Aug. 2024.

[51] R. Zhang, L. Cheng, S. Wang, Y. Lou, W. Wu, and D. W. K. Ng, "Tensor decomposition-based channel estimation for hybrid mmWave massive MIMO in high-mobility scenarios," *IEEE Trans. Commun.*, vol. 70, no. 9, pp. 6325–6340, Sep. 2022.

[52] R. Zhang et al., "Channel estimation for movable-antenna MIMO systems via tensor decomposition," 2024, *arXiv:2407.18773*.